**The EMBO Journal (2013) 32,** 1855–1868
www.embojournal.org

TRANSPARENT PROCESS

THE EMBO JOURNAL

# Exonuclease hDIS3L2 specifies an exosome-independent 3′-5′ degradation pathway of human cytoplasmic mRNA

**Michal Lubas[1,2,3,4], Christian K Damgaard[2,5], Rafal Tomecki[3,4,5], Dominik Cysewski[3,4], Torben Heick Jensen[1,2,*] and Andrzej Dziembowski[3,4,*]**

[1]Centre for mRNP Biogenesis and Metabolism, Aarhus University, Aarhus C, Denmark, [2]Department of Molecular Biology and Genetics, Aarhus University, Aarhus C, Denmark, [3]Department of Biophysics, Institute of Biochemistry and Biophysics, Polish Academy of Sciences, Warsaw, Poland and [4]Department of Genetics and Biotechnology, Faculty of Biology, University of Warsaw, Warsaw, Poland

**Turnover of mRNA in the cytoplasm of human cells is thought to be redundantly conducted by the monomeric 5′-3′ exoribonuclease hXRN1 and the 3′-5′ exoribonucleolytic RNA exosome complex. However, in addition to the exosome-associated 3′-5′ exonucleases hDIS3 and hDIS3L, the human genome encodes another RNase II/R domain protein—hDIS3L2. Here, we show that hDIS3L2 is an exosome-independent cytoplasmic mRNA 3′-5′ exonuclease, which exhibits processive activity on structured RNA substrates *in vitro*. hDIS3L2 associates with hXRN1 in an RNA-dependent manner and can, like hXRN1, be found on polysomes. The impact of hDIS3L2 on cytoplasmic RNA metabolism is revealed by an increase in levels of cytoplasmic RNA processing bodies (P-bodies) upon hDIS3L2 depletion, which also increases half-lives of investigated mRNAs. Consistently, RNA sequencing (RNA-seq) analyses demonstrate that depletion of hDIS3L2, like downregulation of hXRN1 and hDIS3L, causes changed levels of multiple mRNAs. We suggest that hDIS3L2 is a key exosome-independent effector of cytoplasmic mRNA metabolism.**

*The EMBO Journal* (2013) **32,** 1855–1868. doi:10.1038/emboj.2013.135; Published online 11 June 2013
*Subject Categories:* RNA
*Keywords*: hDIS3L2; P-bodies; ribonuclease; RNA decay; Xrn1

## Introduction

Synthesis and degradation rates control steady-state levels of RNA in all organisms. In eukaryotes, the newly synthesized mRNA is challenged by quality control mechanisms ensuring that only efficiently processed molecules are exported to the cytoplasm to undergo multiple rounds of translation before their decay (Houseley and Tollervey, 2009; Muhlemann and Jensen, 2012). The cytoplasmic stability of mRNA is determined by multiple factors with the rate-limiting step usually being poly(A) tail shortening by deadenylation (Decker and Parker, 1993; Muhlrad *et al*, 1994; Korner and Wahle, 1997; Goldstrohm and Wickens, 2008). In *S. cerevisiae*, this is mainly achieved by the evolutionary conserved CCR4-NOT complex, while in humans the PAN2/PAN3 deadenylase is also involved in the initial stages of the process (Korner and Wahle, 1997; Goldstrohm and Wickens, 2008). Shortened mRNA poly(A) tails lose their interaction with poly(A) tail-binding proteins (PABPs), which leads to the activation of either 5′-3′ or 3′-5′ directional decay. In *S. cerevisiae*, the former pathway is initiated by Lsm1-7p complex-stimulated decapping by Dcp2p followed by 5′-3′ exonucleolytic attack by Xrn1p (Stevens, 1980; Decker and Parker, 1993; Muhlrad *et al*, 1994; Geisler and Coller, 2012), while the latter depends on the major 3′-5′ exoribonuclease, the RNA exosome (Mitchell *et al*, 1997; Anderson and Parker, 1998; Houseley and Tollervey, 2009; Lubas *et al*, 2012). Although less explored, homologous degradation factors are believed to predominate in the cytosol of human cells. Here, one of the best-studied decay pathways is that of unstable mRNAs, containing AU-rich elements (AREs) in their 3′ UTRs. AREs are recognized by specific proteins, which in turn attract degradation factors, including the human homologue of Xrn1p, hXRN1, and the RNA exosome complex (Schoenberg and Maquat, 2012).

While mRNA decay has been reported to occur on polysomes (Hu *et al*, 2009; Hu *et al*, 2010), studies have also revealed that non-translating mRNA can aggregate into cytoplasmic ribonucleo-protein (RNP) granules, so-called P-bodies (PBs), that store mRNA and/or facilitate its degradation (Decker and Parker, 2012). Decapping factors, Xrn1 and other conserved decay factors, but not RNA exosome subunits, often accumulate in PBs (Sheth and Parker, 2003; Cougot *et al*, 2004; Fenger-Gron *et al*, 2005). Depletion or inactivation of Dcp2 or Xrn1 enhances PB formation, suggesting that an excess of non-degraded mRNA nucleates PBs when this major mRNA decay pathway is blocked (Sheth and Parker, 2003; Cougot *et al*, 2004; Fenger-Gron *et al*, 2005; Franks and Lykke-Andersen, 2008). Under normal conditions, PBs are not essential for cytoplasmic mRNA decay (Eulalio *et al*, 2007), possibly since Dcp1/2 and Xrn1 are already present on polysomes (Mangus and Jacobson, 1999; Wang *et al*, 2002; Hu *et al*, 2009). Besides such constitutive turnover, regulated mRNA decay pathways, involving endonucleolytic cleavage or destabilizing *cis* elements (Balagopal *et al*, 2012; Schoenberg and Maquat, 2012), can also occur on polysomes (Hu *et al*, 2010). In contrast, exosome-mediated degradation has not been coupled to eukaryotic translation.

*Corresponding authors. TH Jensen, Department of Molecular Biology and Genetics, Aarhus University, C.F. Møllers Allé 3, Building 1130, 8000 Aarhus C, Denmark. Tel.: +45 60202705; Fax: +45 86196500; E-mail: thj@mb.au.dk or A Dziembowski, Department of Biophysics, Institute of Biochemistry and Biophysics, Polish Academy of Sciences, ul. Pawinskiego 5a, Warsaw 02-106, Poland. Tel.: +48 225922033; Fax: +48 226584176; E-mail: andrzejd@ibb.waw.pl
[5]These authors contributed equally to this work

**Received: 1 November 2012; accepted: 15 May 2013; published online: 11 June 2013**

The *S. cerevisiae* exosome consists of a catalytically inert nine-subunit ring structure with a central channel and associated catalytic subunits: the ubiquitously present endo-/exo-nuclease Dis3p and the nucleus-restricted 3′-5′ exonuclease Rrp6p (Allmang *et al*, 1999; Dziembowski *et al*, 2007; Lebreton *et al*, 2008). Dis3p harbours a catalytic ribonuclease II-like (RNB) domain, responsible for the processive exonuclease activity, supported by three RNA-binding domains of the oligonucleotide binding (OB) fold. Dis3p also displays endonucleolytic activity that derives from the PilT N-terminus (PIN) domain (Lebreton *et al*, 2008; Schaeffer *et al*, 2009, 2012; Schneider *et al*, 2009). In addition to its catalytic activity, the PIN domain, together with the upstream-located zinc-binding CR3 motif, is responsible for the association of Dis3p with the exosome core through interaction with the Rrp41p subunit. Both nucleolytic activities of Dis3p are controlled by the exosome core, since RNA is threaded through the central exosome channel to reach the Dis3p catalytic sites (Bonneau *et al*, 2009; Wasmuth and Lima, 2012; Drazkowska *et al*, 2013; Makino *et al*, 2013). The exosome complex in human cells has diversified, as it is found in at least three compartment-specific isoforms: a nucleolar, a nucleoplasmic (non-nucleolar), and a cytoplasmic one (Staals *et al*, 2010; Tomecki *et al*, 2010; Lykke-Andersen *et al*, 2011). Moreover, unlike *S. cerevisiae*, mammalian cells possess two homologues of the Dis3p protein: hDIS3, which is enriched in the nucleoplasm and hDIS3-Like (hDIS3L), which is exclusively cytoplasmic. The third catalytic exosome subunit, hRRP6, is mainly nuclear/nucleolar with a minor cytoplasmic localization (Schilders *et al*, 2007). Curiously, although hDIS3L has lost endonucleolytic activity, it still associates with the exosome core through its catalytically inert N-terminal PIN domain. Thus, exosome-dependent 3′-5′ decay in the mammalian cytosol has diverged from that of the *S. cerevisiae* system by eliminating endonucleolytic activity thought to assist in the degradation of structured substrates (Lebreton *et al*, 2008). In addition to hDIS3 and hDIS3L, the human genome encodes a third putative Dis3p homologue—hDIS3-Like2 (hDIS3L2). The N-terminus of hDIS3L2 is only weakly conserved and lacks a detectable PIN domain, questioning whether this protein functions in the context of the exosome core. Recently, mutations in the *hDIS3L2* gene have been found among patients with Perlman syndrome-congenital overgrowth disease and Wilms' tumour susceptibility (Astuti *et al*, 2012). These mutations were suggested to inhibit the exonucleolytic activity of hDIS3L2 and lead to deregulation of cell-cycle genes resulting in faster cell growth. Nevertheless, the molecular basis underlying such pathogenesis as well as the more general cellular function of hDIS3L2 remains uncharacterized.

Here, we report an *in vitro* and *in vivo* characterization of hDIS3L2. We provide evidence that hDIS3L2 is an exosome-independent RNase and define its exonucleolytic properties. hDIS3L2-depletion effects are compared to those of depleting two other key cytoplasmic ribonucleases: hXRN1 and hDIS3L, demonstrating substantial alterations in bulk mRNA levels, with stronger effects observed upon hDIS3L2 and hXRN1 depletions. Finally, we show that hDIS3L2 targets a general class of mRNA, the ARE-containing transcripts. Thus, hDIS3L2 is a key effector of human cytoplasmic 3′-5′ decay of mRNA.

## Results

### *hDIS3L2 is an exosome-independent cytoplasmic ribonuclease*

The human genome encodes three homologues of Dis3p: hDIS3, hDIS3L, and hDIS3L2 (Staals *et al*, 2010; Tomecki *et al*, 2010). Both hDIS3 and hDIS3L possess all Dis3 family domains, namely the cold shock domains (CSDs), the RNB domain and the S1 domain, also present in bacterial RNase II/R, as well as the N-terminal PIN domain and zinc-binding CR3 motif (Figure 1A; Supplementary Figure S1A) (Lebreton *et al*, 2008; Schaeffer *et al*, 2012). In contrast, hDIS3L2 lacks the CR3 and PIN regions. Moreover, its first RNA-binding CSD domain (CSD1) is extended, a feature only conserved among hDIS3L2 proteins (Supplementary Figure S1A). Phylogenetic analysis indicates that hDIS3L2 is quite divergent from other members of the Dis3 family and widespread among other phyla (Supplementary Figure S1B). Besides hDIS3L2, the only orthologue described so far is the plant ribonuclease SOV, which functions in cytoplasmic RNA decay and becomes essential in the absence of the decapping scaffold protein VCS (plant homologue of human HEDLS/EDC4) (Zhang *et al*, 2010).

Since structural and functional data from *S. cerevisiae* have shown that the N-terminus of Dis3p anchors it to the exosome core (Bonneau *et al*, 2009; Schneider *et al*, 2009; Schaeffer *et al*, 2012), the absence of a corresponding region in hDIS3L2 questioned whether such association occurs in this case. To clarify this, we performed co-immunoprecipitation (coIP) analyses of C-terminally FLAG-tagged hDIS3, hDIS3L, and hDIS3L2 fusion proteins stably expressed in HEK293 (Flp-In T-Rex) cell lines. The coIP lysis buffer was supplemented with RNase A in order to avoid detection of RNA-mediated interactions. In agreement with previously reported data (Staals *et al*, 2010; Tomecki *et al*, 2010; Lubas *et al*, 2011), western blotting analysis using antibodies against hRRP40 and hRRP6 demonstrated the presence of these components in the eluates of both hDIS3 and hDIS3L co-precipitates (Figure 1B, note the minor presence of hRRP6 in the hDIS3L coIP, consistent with the cytoplasmic localization of hDIS3L). In contrast, high amounts of purified hDIS3L2 did not co-precipitate any detectable quantities of neither hRRP40 nor hRRP6. Thus, it is unlikely that hDIS3L2 interacts with the exosome core.

We next determined the intracellular localization of hDIS3L2. Since available antibodies against the endogenous protein were not suitable for immunofluorescence studies, we analysed HEK293 stably expressing hDIS3L2-FLAG or cells transiently transfected with C- or N-terminal EGFP fusions of hDIS3L2 (Figure 1C, top panels and data not shown). In addition, we carried out live cell confocal microscopy of HeLa cells transiently expressing hDIS3L2-EGFP (Figure 1C, middle panels). In all tested cases, hDIS3L2 localized exclusively to the cytoplasm, showing a homogenous distribution throughout this compartment. Since the plant SOV protein was reported to localize in cytoplasmic foci and since a granular localization is also compatible with a previous localization study of the human protein (Zhang *et al*, 2010; Astuti *et al*, 2012), we also produced polyclonal antibodies to be able to localize endogenous hDI3L2 present at physiological levels. Using this new reagent, the protein was again evenly distributed in the cytoplasm of HeLa cells (Figure 1C, bottom

 

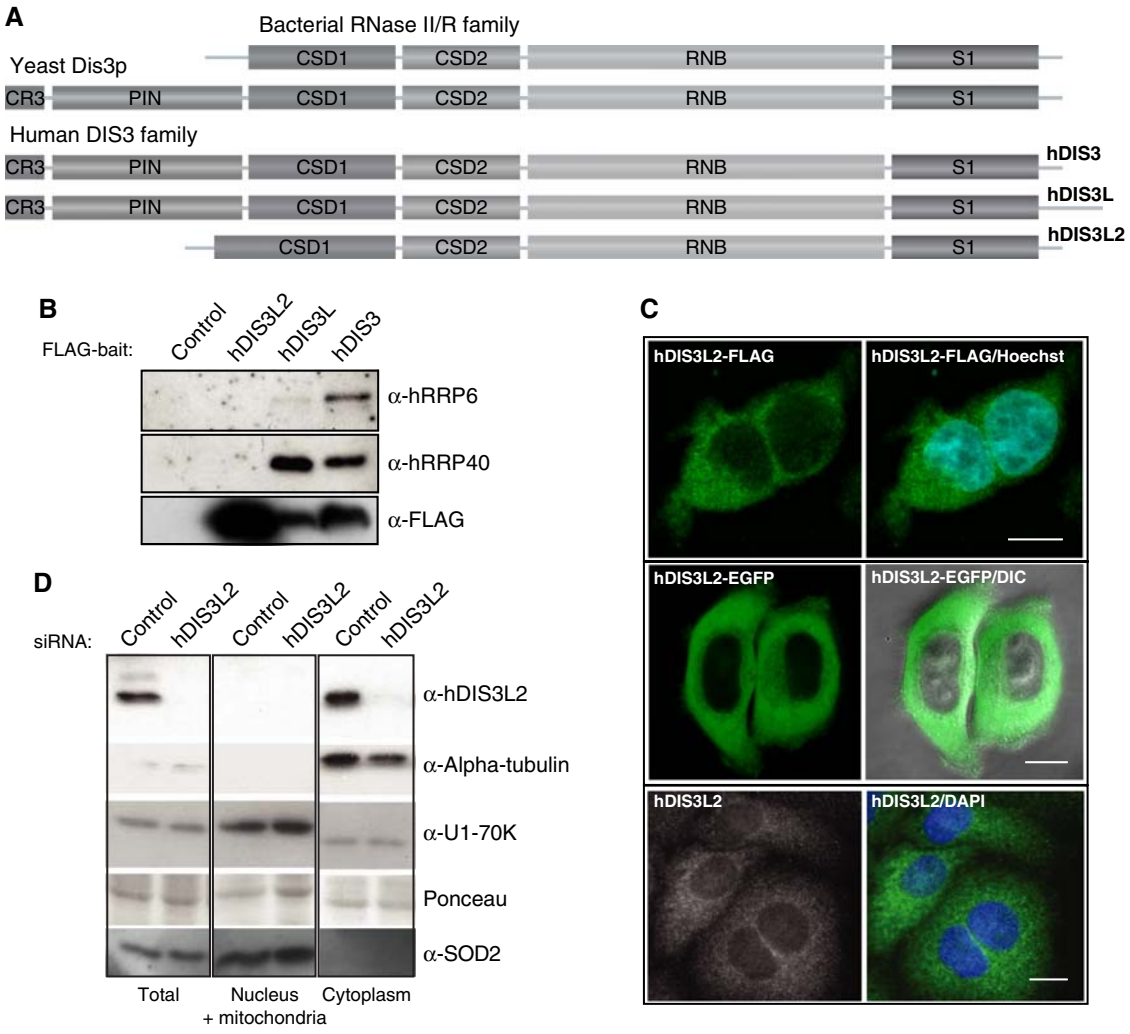


**Figure 1** hDIS3L2 is an RNase II/R family-related and exosome-independent factor. (**A**) Domain composition of hDIS3L2 and its homologues. The RNB domain and the three RNA-binding domains (CSD1, CSD2, and S1) are present in all proteins. In contrast, the PIN domain and the CR3 motif are features characteristic for the Dis3 family, and absent from hDIS3L2, which instead harbours an extended CSD1 domain. (**B**) CoIP/western blotting analysis of hDIS3L2, hDIS3L, and hDIS3 associations with exosome subunits. hDIS3L2-, hDIS3L-, and hDIS3-FLAG IP eluates were probed with antibodies against hRRP6, hRRP40, and FLAG peptide as indicated. An empty host cell line was used as a negative control. (**C**) Subcellular localization analysis of hDIS3L2 in HEK293 (top) and HeLa (middle and bottom) cells. HEK293 Flp-In T-Rex cells were stably expressing C-terminal FLAG-tagged hDIS3L2, which was visualized by fluorescence microscopy. In the middle panel, HeLa cells were transiently transfected with a construct encoding hDIS3L2-EGFP, directly analysed by live-cell confocal microscopy and overlaid with phase contrast. The endogenous hDIS3L2 was detected in HeLa cells with rabbit α-hDIS3L2 antibodies (bottom). Blue colour indicates nuclei, stained with Hoechst or DAPI. Scale bars indicate 100 μm. (**D**) Analysis of hDIS3L2 distribution by subcellular fractionation of HeLa cells. Protein equivalents of total, nucleus/mitochondria, and cytoplasmic cell fractions were analysed by SDS–PAGE followed by western blotting analysis using α-hDIS3L2, α-alpha-tubulin (cytoplasmic marker), α-U1-70K (nuclear marker), and α-SOD2 (mitochondrial marker) antibodies as indicated. Ponceau staining was performed as a loading control.

panels). Finally, to verify the immunolocalization analyses and to also exclude a possible mitochondrial localization of hDIS3L2, we fractionated control, or hDIS3L2-depleted HeLa cells using digitonin and subjected total, nuclear/mitochondrial and cytoplasmic fractions to hDIS3L2 western blotting analysis. This experiment confirmed hDIS3L2 cytoplasmic enrichment as well as its nuclear and mitochondrial exclusion (Figure 1D).

### *hDIS3L2 is a processive 3′-5′ exonuclease, which can efficiently degrade structured substrates*

Having established its exosome independence, we next wanted to assess the biochemical properties of hDIS3L2. To this end, we expressed in *E. coli*, and purified to near-homogeneity (Supplementary Figure S2A), full-length wild-type protein (hDIS3L2$^{WT}$) and its counterpart with a mutation in the RNB domain (hDIS3L2$^{mut}$), in which a conserved aspartic acid residue predicted to coordinate a divalent cation was replaced by asparagine (D391N) (Supplementary Figure S1A). Ribonuclease activities of ion exchange chromatography fractions correlated with the peak of hDIS3L2$^{WT}$ presence (Supplementary Figure S2B), and was absent from the hDIS3L2$^{mut}$ purification (Supplementary Figure S2C). Subsequent nuclease assays were carried out in conditions previously used for yeast and human Dis3 proteins (Lorentzen *et al*, 2008; Tomecki *et al*, 2010). Efficient substrate degradation was observed over a broad concentration spectrum of magnesium and manganese ions

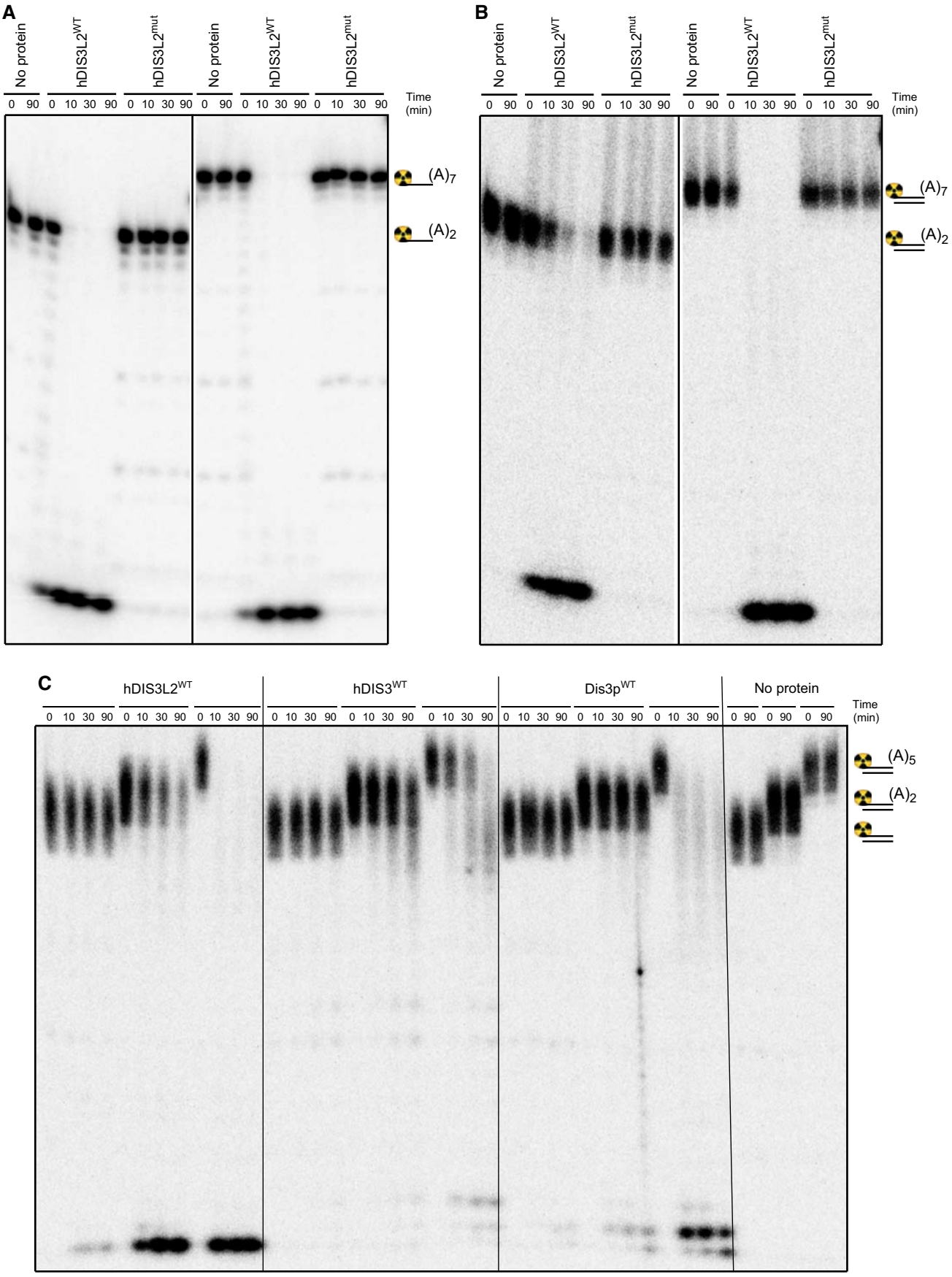

(40 μM to 1 mM), but was inhibited by zinc ions at a 200-μM concentration (Supplementary Figure S1D). Using 5′end radiolabelled single-stranded (ss): 19-mer ($A_2$-tail), 22-mer ($A_5$-tail), 24-mer ($A_7$-tail) and 31-mer ($A_{14}$-tail) RNA substrates, we were able to obtain clear evidence for the predicted processive hDIS3L2 3′-5′ exonucleolytic activity, which strictly depended on the presence of the D391 catalytic site residue (Figure 2A; Supplementary Figure S2C and E). The hDIS3L2 protein degraded the ssRNA substrates with an efficiency comparable to that of wild-type hDIS3 ($hDIS3^{WT}$), but curiously, hDIS3L2 released shorter degradation products (3 nt), than hDIS3 (4–5 nt) (Supplementary Figure S2F and G) (Lorentzen *et al*, 2008; Tomecki *et al*, 2010). This 3′-5′ degradation pattern is more similar to bacterial RNase R, which releases 2–3 nt end products (Cheng and Deutscher, 2002).

Given the fact that Dis3 and RNase R proteins have the ability to unwind double-stranded (ds) structures (Lorentzen *et al*, 2008; Lee *et al*, 2012), we also tested this putative property of hDIS3L2 using 17-mer dsRNAs with 2, 5, 7, or 14 nt 3′adenosine overhangs, labelled at the 5′-end of the respective 3′-extended strands. hDIS3L2 very efficiently unwound and degraded RNA duplexes provided that some 3′ssRNA extension was present (Figure 2B and C; Supplementary Figure S2H). We then compared the activity of hDIS3L2 to those of its yeast and human Dis3 homologues. To our surprise, hDIS3L2 was significantly less sensitive to the length of 3′ssRNA extension and to a minor extent also accessed completely blunt dsRNA (Figure 2C). In the cases of hDIS3 and Dis3p, only the substrates with extensions of sufficient length (5 nt) were prone to degradation. Moreover, hDIS3L2 degraded the structured substrates more rapidly than hDIS3 or Dis3p. This observed efficiency of dsRNA degradation by hDIS3L2 suggests that its RNA-binding site may reside narrowly within the enzyme's active site. Alternatively, the extended CSD1 of hDIS3L2 may improve its unwinding ability, perhaps due to the different spatial arrangement of the OB-fold RNA-binding domains. Further structural and biochemical studies are needed to explain the observed differences in biochemical properties of various eukaryotic RNaseII/R family members.

Finally, since the existence of a PIN-like domain in hDIS3L2 has been suggested (Staals *et al*, 2010), we also assayed for any potential additional nucleolytic activity of the enzyme. This was performed using both a circular RNA substrate and a 22-nt ssRNA with two ribonuclease-resistant thymidine nucleotides at its 3′end. No traces of neither endo- nor 5′-3′ exo-nucleolytic activity were detected (Supplementary Figure S2I and J). We conclude that hDIS3L2 is an active 3′-5′ exonuclease with catalytic properties similar to those of the bacterial RNaseII/R family of enzymes.

### *hDIS3L2 associates with hXRN1 and polysomes*

Moving on to the characterization of *in vivo* functions of hDIS3L2, we first used HEK293 cells stably expressing hDIS3L2-FLAG, and empty control cells, to conduct coIP's followed by mass-spectrometry (MS) analysis of the eluates. Experiments were performed either in the presence of RNase A and divalent ions (2.5 mM $MgCl_2$) or under conditions preserving RNA-dependent interactions, that is, without RNase and in the presence of 2 mM EDTA. Proteins remaining on anti-FLAG agarose beads after washes with low stringency buffers were eluted with FLAG peptide and subjected to liquid chromatography-MS (LC-MS) with subsequent quantification analysis using MaxQuant against the Uniprot database (Supplementary Table S1). Consistent with our previous western blotting analysis (Figure 1B), no exosome subunit peptides were detected over background in either condition (Supplementary Table S1). However, interestingly, hDIS3L2 was found to co-purify with the major cytoplasmic 5′-3′ exonuclease hXRN1 in an RNA-dependent manner, a result recapitulated by western blotting analysis of the eluates (Figure 3A). Indeed, hXRN1 was the only significant hit repetitively found in the IP/MS analyses.

In some coIP experiments, peptides corresponding to ribosomal proteins and translation factors were enriched. However, as many of these were also found in 'bead proteome' control IPs (Tomecki *et al*, 2010; Lubas *et al*, 2011), they were not considered as specific hDIS3L2 interactors. Still, to address whether hDIS3L2 can associate with translating ribosomes, we used sucrose density gradients (10–50%) to separate these from HeLa cell extract, and assessed fractions for potential co-sedimenting cytoplasmic degradation factors. As expected, hXRN1, which can initiate mRNA degradation co-translationally (Hu *et al*, 2009), was found to sediment with ribosomal monosomes and polysomes (Figure 3B, top panel). Importantly, the hDIS3L2 fractionation profile resembled that of hXRN1, whereas the hRRP40 exosome subunit was not found in these fractions. Such hDIS3L2-containing heavy complexes indeed represent *bona fide* polysomes, since omission of cycloheximide and inclusion of EDTA, which efficiently collapses polysomes, shifted both hXRN1 and hDIS3L2 into light fractions (Figure 3B, bottom panel). The presence of hDIS3L2 in the polysomal fractions is surprising because 3′-5′ degradation activities, other than deadenylases, have not previously been connected to the translation process. Nevertheless, our results suggest that hDIS3L2 and hXRN1 may, at least partly, cooperate in the degradation of mRNA already during translation. This notion is in line with the homogenous distribution of hDIS3L2, suggesting that it plays a role outside of cytoplasmic RNA aggregates.

**Figure 2** hDIS3L2 is a processive 3′-5′ exonuclease active towards both ss- and ds-RNA. (**A**) hDIS3L2 displays 3′-5′ exoribonuclease activity towards ssRNA. Wild-type ($hDIS3L2^{WT}$) or mutated ($hDIS3L2^{mut}$) proteins were incubated in the presence of $Mg^{2+}$ ions with 5′radiolabelled single-stranded 17nt RNA oligonucleotide substrates bearing oligoadenosine extensions of different length ($A_2$ or $A_7$) (see also Supplementary Figure S2E). Control reactions were performed in the absence of added protein (no protein). Reactions were terminated at the indicated time points and the products were analysed by 20% acrylamide/7 M urea PAGE followed by phosphorimaging. (**B**) hDIS3L2 is active towards dsRNA. RNase assays were performed as in **A**, but using 5′radiolabelled partially structured double-stranded 17nt RNA substrates in which the longer (labelled) oligoribonucleotide possessed 3′ss oligoadenosine overhangs of different length ($A_2$ or $A_7$) (see also Supplementary Figure S2H). (**C**) hDIS3L2 degrades partially structured RNA substrates bearing short single-stranded extensions more efficiently than hDIS3 and yeast Dis3p. Equal amounts of wild-type recombinant hDIS3L2, hDIS3 or *S. cerevisiae* Dis3p proteins were used for RNase assays performed as in **B** using radiolabelled blunt double-stranded 17nt RNA substrate or its counterparts with 3′ss oligoadenosine overhangs ($A_2$ or $A_5$).

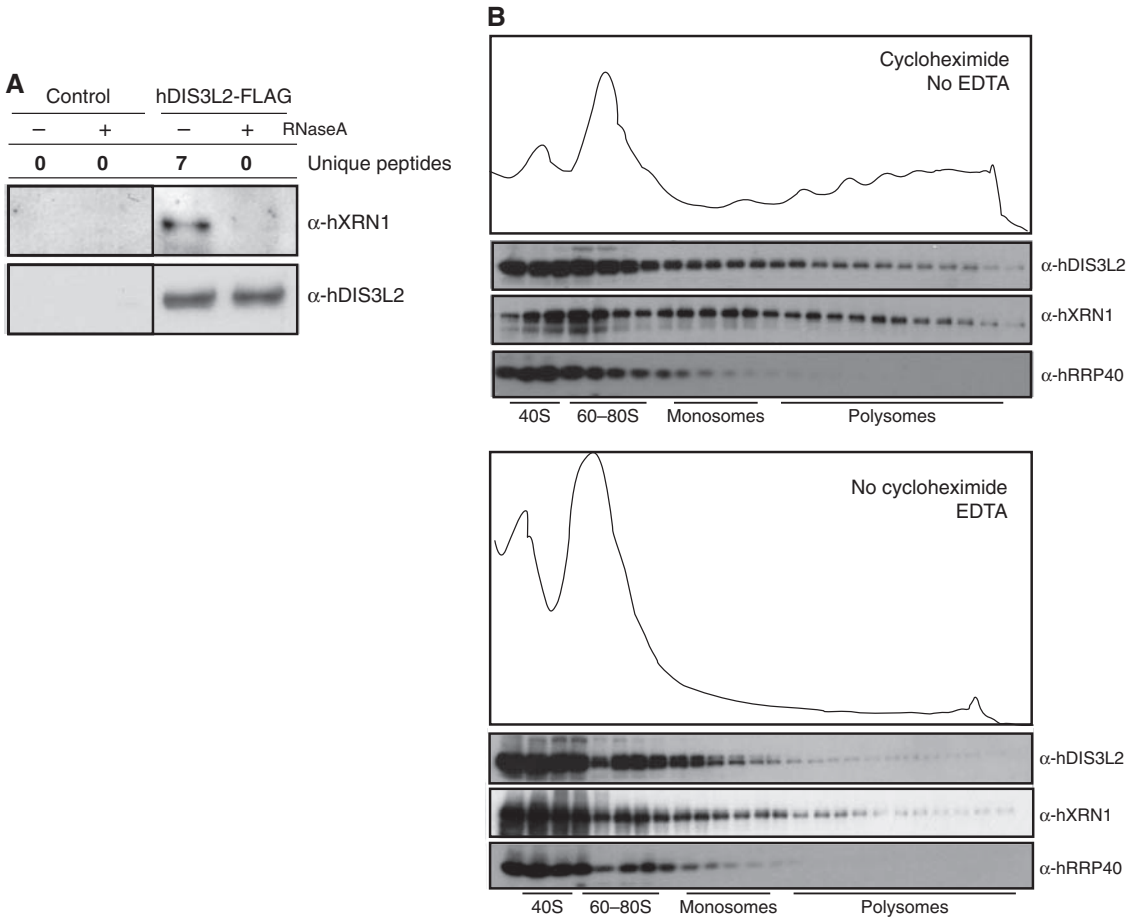


**Figure 3** hDIS3L2 interacts RNA dependently with hXRN1 and co-sediments with translating ribosomes. (**A**) In the presence of RNA, hXRN1 was detected as a specific interaction partner of hDIS3L2-FLAG as assayed by coIP/MS and coIP/western blotting analysis. MS results are shown as unique peptide counts from a representative biological replicate. For full data sets, see Supplementary Table S1. For IP/western blotting analysis, control (empty host cell line) and tetracycline-induced cell extracts were lysed in a buffer with or without RNAse A as indicated. Eluates from anti-FLAG columns were analysed by western blotting using α-hDIS3L2 and α-hXRN1 antibodies. (**B**) Both hDIS3L2 and hXRN1 co-purifies with polysomes. HeLa cells were treated with cycloheximide and subjected to 10–50% sucrose gradient fractionation followed by examination of the abundance of translating ribosomes (see Materials and methods). Collected fractions were analysed by western blotting using α-hXRN1, α-hDIS3L2, and α-hRRP40 antibodies as indicated. The bottom panel shows the control of disrupting polysomes. The sucrose gradient was performed in the absence of cycloheximide and in the presence of 12.5 mM EDTA. The five first fractions were diluted 2-fold prior to SDS–PAGE analysis.

### *hDIS3L2 depletion increases PB frequency*

Given our findings that hDIS3L2 is a *bona fide* cytoplasmic exonuclease, that precipitates with hXRN1 in the presence of RNA, we surmised that hDIS3L2 activity would be generally active towards bulk cytoplasmic mRNA. To address this possibility, we took advantage of the notion that inactivation of either of the cytoplasmic decay enzymes hXRN1 or hDCP2 enhances PB formation, consistent with nucleation of PB factors on excess mRNA (Sheth and Parker, 2003; Cougot *et al*, 2004; Fenger-Gron *et al*, 2005; Franks and Lykke-Andersen, 2007, 2008). We therefore asked what would be the impact of hDIS3L2 depletion (Supplementary Figure S3A) on the number and morphology of PBs. In addition, we also depleted hXRN1 (Supplementary Figure S3A) or hDIS3L (Supplementary Figure S3B), the latter of which was chosen as a strictly cytoplasmic exosomal subunit (Tomecki *et al*, 2010). Since decapping factors are among the many RNA-binding proteins constituting PBs, we monitored the localization of endogenous hDCP1a as a marker for these. Interestingly, hDIS3L2 depletion resulted in a significantly increased number of PBs (Figure 4A, compare 'control' to 'hDIS3L2'; quantified in Figure 4B). A similar effect was observed when using antibodies against hXRN1 as a marker for PBs (Supplementary Figure S3C). The depletion of hXRN1 led to a increase in the sizes of PBs without a strong effect on their numbers (Figure 4A and B, compare 'control' to 'hXRN1'), suggesting accumulation of stabilized RNAs within these foci. In contrast, hDIS3L depletion had no detectable effect on PB number or morphology (Figure 4A and B). To extend these observations, we also performed double depletions of hXRN1 with either hDIS3L or hDIS3L2. While the phenotypic consequence of co-depleting hDIS3L was negligible, co-depletion of hDIS3L2 with hXRN1 resulted in a compound effect of the individual knockdowns (see Discussion). Though indirect, these data provide support for a key role of hDIS3L2 in bulk cytoplasmic mRNA decay.

PB sizes/numbers are proportional to the amount of non-translating mRNA. Treatment of cells with translation elongation drugs, such as emetine, 'traps' mRNA on polysomes and leads to a decrease in the non-translating mRNA

 

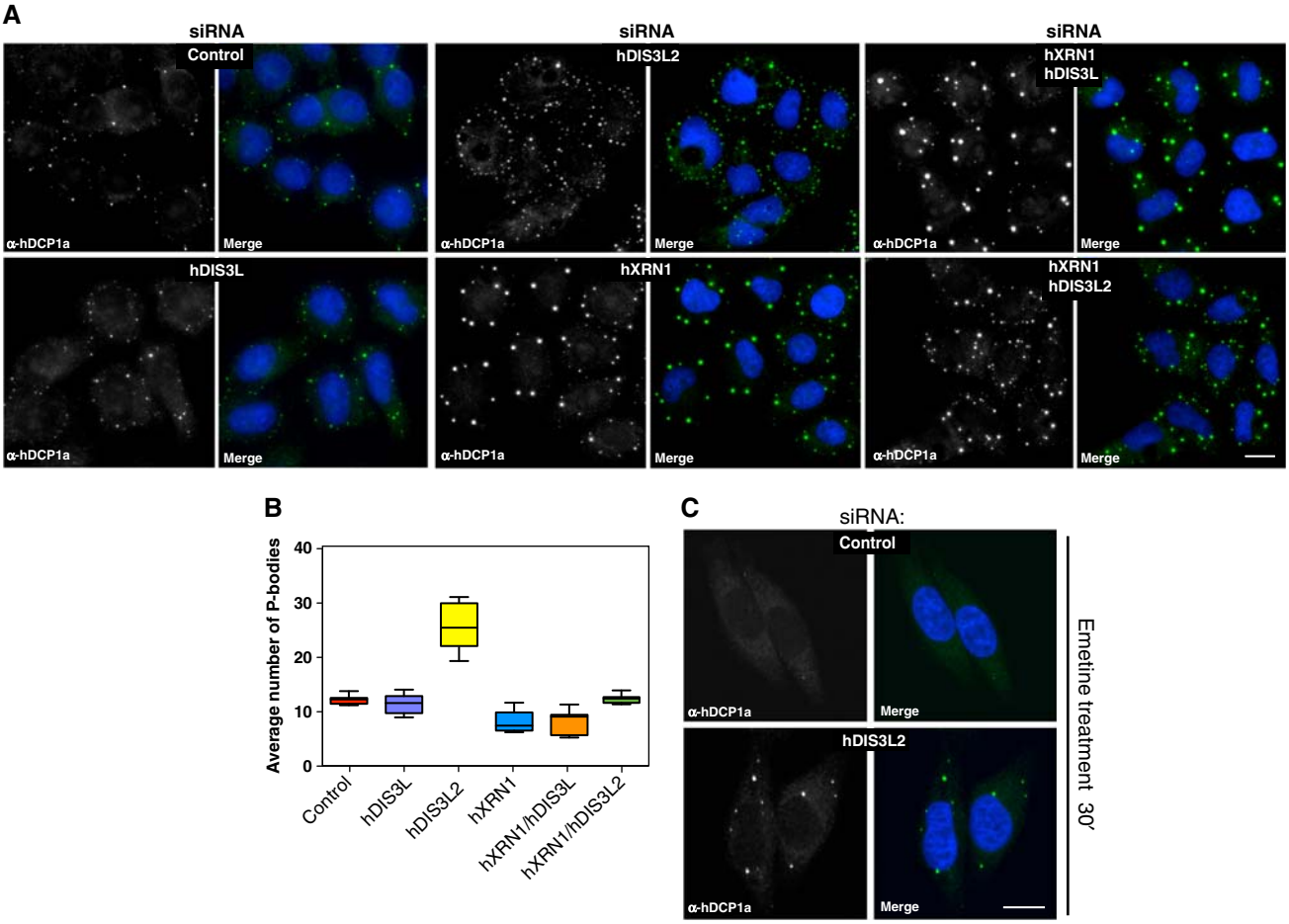


**Figure 4** hDIS3L2 depletion increases the numbers of PBs. (**A**) hDCP1a staining as a PB proxy of cells treated with siRNA against EGFP (control), hDIS3L, hDIS3L2, hXRN1, hXRN1/hDIS3L, or hXRN1/hDIS3L2 as indicated. Cells were inspected by fluorescence microscopy using a ×40 objective. Nuclei were stained with DAPI and merged with protein staining as indicated. Scale bar indicates 100 μm. (**B**) Boxplots displaying the average number of PBs per siRNA-treated cell from **A**. In all, 150 cells were inspected per experiment. Boxes indicate 5th and 95th percentiles, while thick lines indicate the mean values. (**C**) EGFP (control) or hDIS3L2 siRNA-treated HeLa cells subjected to 30 min emetine treatment to inhibit translation elongation. Cells were fixed and stained with α-hDCP1a antibodies. Control cells showed a decreased number of PBs while a 40% fraction of hDIS3L2-depleted cells retained PBs upon emetine treatment. Scale bar indicates 100 μm.

pool with a consequential loss of visible PBs (Kedersha *et al*, 2005; Franks and Lykke-Andersen, 2008). To strengthen the observed phenotypic effect on PBs upon hDIS3L2 depletion, we therefore treated cells with emetine in the presence or absence of siRNA directed against hDIS3L2. Previous evidence suggests that depletion of decapping enzymes, or hXRN1, renders PBs unaffected by emetine treatment (Franks and Lykke-Andersen, 2008), presumably because the load of non-translating mRNA remains high in the absence of 5′-3′ decay. Upon hDIS3L2 knockdown, hDCP1a-positive PBs persisted during emetine treatment (Figure 4C, compare with Figure 4A), providing further support that hDIS3L2 is important for general mRNA turnover.

### *hDIS3L2 contributes to the maintenance of cellular RNA homeostasis*

To directly assess the effect of hDIS3L2 downregulation on mRNA levels, we first focused on the class of ARE-containing transcripts (Chen and Shyu, 1995; Chen *et al*, 2001; Stoecklin *et al*, 2006). ARE-mRNAs accumulate in PBs (Franks and Lykke-Andersen, 2007) and have very short half-lives (Lykke-Andersen and Wagner, 2005; Stoecklin *et al*, 2006; Franks and Lykke-Andersen, 2007). Hence, β-globin reporter constructs, containing the TNF-α ARE (β-TNF-α), or a control 3′UTR sequence from GAPDH (β-GAPDH), in their 3′UTRs were transfected into HeLa Tet-off cells treated with siRNA against EGFP or hDIS3L2. β-TNF-α mRNA levels were subsequently measured in a tetracycline pulse-chase time course by northern blotting analysis. This approach revealed that depletion of hDIS3L2 affected ARE-mediated decay (AMD) by increasing the half-life of the β-TNF-α RNA by ∼2-fold (Figure 5). These results provide the first direct evidence for an *in vivo* RNase activity of hDIS3L2 in higher eukaryotes. Similar effects on AMD were previously reported for depletion of either hXRN1 or various subunits of the exosome complex (Stoecklin *et al*, 2006), suggesting that ARE-containing transcripts are turned over by overlapping decay pathways.

Next, we aimed to obtain a genome-wide view of the effects of hDIS3L2 depletion on cellular RNA metabolism and to compare it with the depletion of other cytoplasmic exonucleases. We therefore performed duplicate 100 bp RNA-

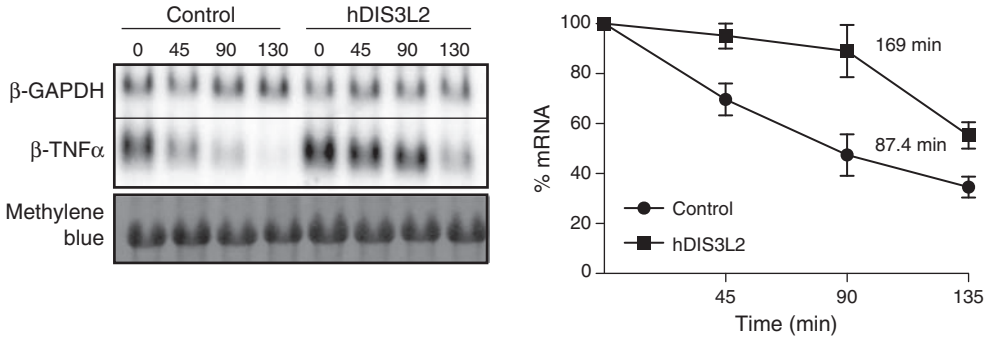


**Figure 5** hDIS3L2 is required for ARE-mediated decay. Half-life measurements of β-globin reporter mRNA containing a 3′UTR element from TNF-α (ARE) performed in cells treated with siRNA against EGFP (control) or hDIS3L2. Transcription was induced and repressed by a tetracycline pulse-chase assay and RNA levels measured by northern blotting analysis (left panel). The graph shows the calculated decay rates and the average levels of β-TNF-α mRNA plotted over time. Mean values were quantified from three independent biological repeats normalized to the levels of β-GAPDH (internal transfection control) with error bars representing standard errors of the mean (right panel).

seq experiments of total RNA isolated from HeLa cells depleted of hDIS3L2, hXRN1 (Supplementary Figure S4A) or hDIS3L (Supplementary Figure S4B). Random-primed cDNA libraries were generated using the ScriptSeq v2 kit (EpiCentre), which enriches for long RNAs (>200 nt), and sequenced using the Illumina HiScan system. With 13–30 million mapped reads from the various libraries, we determined a comprehensive set of differentially expressed genes (DEGs) using the DESeq software package (Anders and Huber, 2010). A heat map clustering the 200 most significant DEGs by expression revealed differences between the three knockdowns (Supplementary Figure S5A; Supplementary Tables S2–S4), of which hXRN1- and hDIS3L2-depletion samples were clustered closest as shown by a correlation dendrogram (Supplementary Figure S5A, top). The major effects of hDIS3L2 and hXRN1 depletions were displayed in Venn diagrams (Figure 6A; Supplementary Figure S5B), showing 646 and 1003 significantly upregulated mRNAs (>2-fold change, false discovery rate <0.05), respectively, for the two knockdowns. This number was lower, 363, for the hDIS3L depletion consistent with the limited effect of this knockdown on PB count/cell. Most affected transcripts were upregulated; an expected exonuclease depletion phenotype, while some were decreased, most likely representing secondary effects (Supplementary Figure S5B and C). Several affected targets were validated by independent RT-qPCR analysis (Supplementary Figure S5D) and reproduced using a second siRNA against hDIS3L2 (Supplementary Figure S5E). Moreover, we measured relative changes in half-lives of selected mRNAs in control versus DIS3L2-depleted cells using metabolic labelling by 4-thiouridine (4sU) (Dolken *et al*, 2008) (Figure 6D). These analyses confirmed that the selected upregulated transcripts obtain longer half-lives upon hDIS3L2 depletion, demonstrating a direct contribution of this RNase in their decay. In line with our analysis of the β-TNF-α reporter (Figure 5), prominent hDIS3L2 targets were the putative ARE-containing mRNAs: FZD4, E2F7 and ZWINT (ARED3 database; Bakheet *et al*, 2006).

For upregulated transcripts, we did not find any common features, for example, 5′- or 3′-UTR length, sequence composition, or transcript length that would explain their altered levels. We therefore turned to gene ontology (GO) analysis and found in all three depletion experiments an enrichment of upregulated transcripts, which encode proteins involved in cell-cycle regulation and DNA packaging (Figure 6B). Especially, hDIS3L2 and hXRN1 depletions resulted in elevated 'cell-cycle transcripts', whereas the hDIS3L knockdown in particular upregulated histone mRNAs (Supplementary Table S4). Thus, RNA degradation pathways involving hDIS3L2, hDIS3L/exosome, and hXRN1 show significant redundancies. Despite this overlap, some transcripts were upregulated in only one of the three knockdowns (Figure 6A). Of these, GO terms associated with DIS3L2-upregulated targets showed enrichment of mRNAs encoding membrane proteins ($P \leqslant 10^{-9}$), including the endoplasmic reticulum and the Golgi apparatus (Supplementary Figure S5F). For the hXRN1 depletion, non-overlapping transcripts were strongly associated with transcription regulation ($P \leqslant 10^{-14}$) (Supplementary Figure S5F). Thus, different groups of substrates may undergo specific degradation by either of these enzymes.

To extend the analysis of individual knockdowns, we finally prepared libraries from total RNA of double depletions of hXRN1 with either of the two 3′-5′ cytoplasmic exonucleases. As judged by DEGs both double knockdowns yielded synergistic effects and displayed new classes of upregulated transcripts in the GO analyses (Figure 6C). This was most clearly observed for the hDIS3L2/hXRN1 co-depletion; that is, a significant (as indicated by enrichment scores) number of upregulated transcripts mapped to transcription regulation pathways (25% of DEGs) and the cell cycle (8% of DEGs) (Figure 6C; Supplementary Tables S4 and S5). Downregulation of transcripts was also observed upon double depletions, however, only the hDIS3L2/hXRN1 co-depletion revealed GO classes with significant decreases, including mRNAs encoding translation factors (Figure 6C, left).

We conclude that hDIS3L2 and hXRN1 share many targets. Most importantly, our data are consistent with a cytoplasmic hDIS3L2-dependent 3′-5′ RNA degradation pathway that acts in parallel to that of the RNA exosome.

## Discussion

Constitutive turnover of cytoplasmic mRNA in *S. cerevisiae* is initiated by 3′end deadenylation followed by either 3′-5′ degradation by the RNA exosome or 5′-3′ degradation by Xrn1p (Hsu and Stevens, 1993; Muhlrad *et al*, 1994). These two exonucleolytic pathways are largely redundant

 

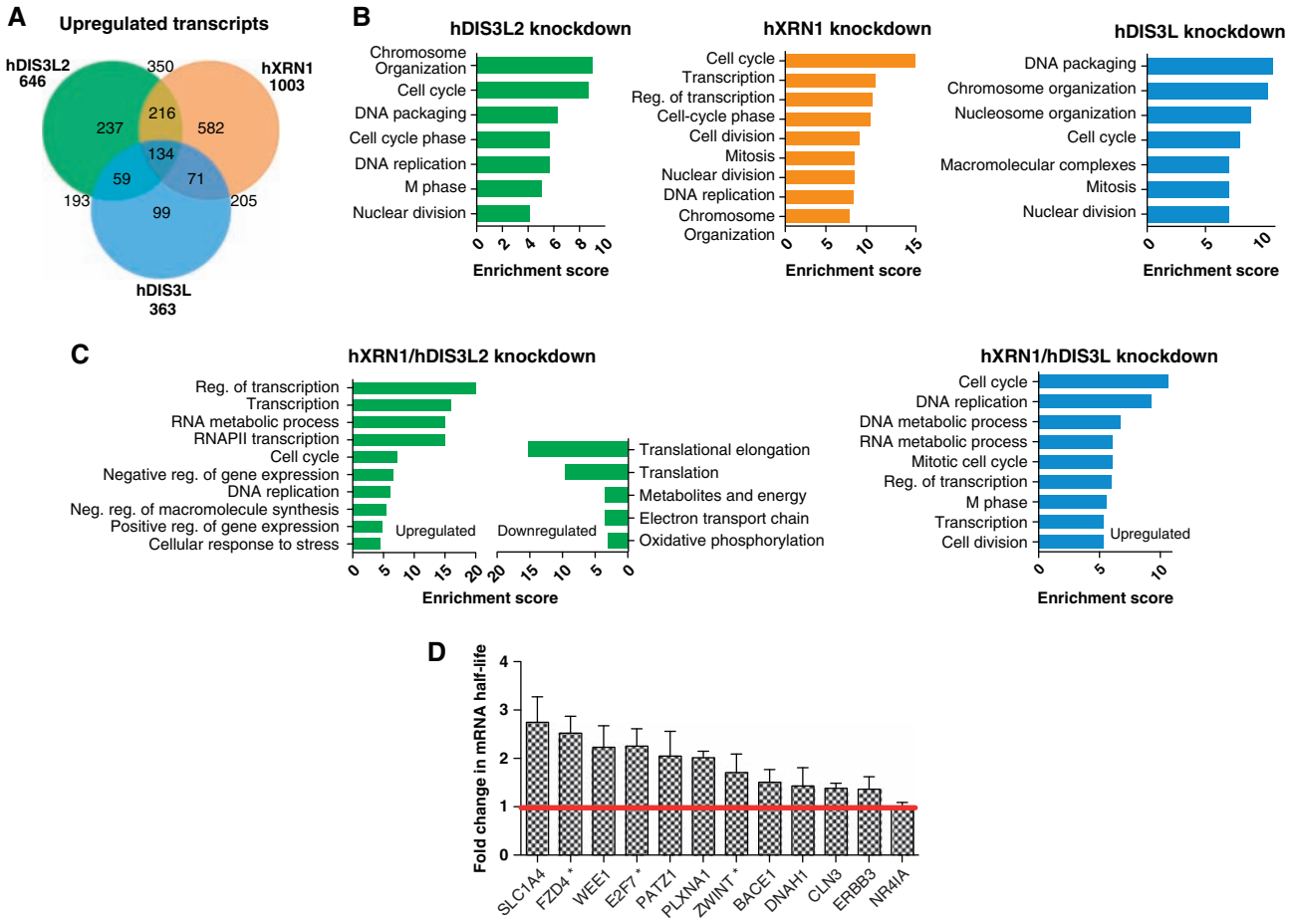


**Figure 6** Transcriptome analysis of hDIS3L2-, hXRN1-, and hDIS3L-depleted cells. (**A**) Venn diagram showing distribution and overlap of upregulated transcripts from hDIS3L2-, hXRN1-, and hDIS3L-depleted cells as identified by DESeq in a given set of biological replicates (for full data sets, see Supplementary Figure S5 and Supplementary Tables S2–S4). Enrichment between sample sets was calculated using hypergeometric test, *P*-values scored below $10^{-30}$. (**B**) GO term analysis of upregulated mRNAs from each knockdown sample versus control clustered using DAVID (false discovery rate $<0.05$). Most enriched clusters for each condition are shown as barplots using enrichment score ($-\log(P\text{-value})$). (**C**) GO term analysis as in **B** for significantly upregulated or downregulated mRNAs from hDIS3L2/hXRN1 and hDIS3L/hXRN1 co-depletions (Supplementary Tables S5 and S6). (**D**) Changes in half-lives of selected mRNA caused by hDIS3L2 siRNA-mediated depletion. Half-lives of mRNAs were determined based on newly transcribed RNA/total RNA ratios (Dolken *et al*, 2008). The EGFP (control) and hDIS3L2 siRNA-treated HeLa cells were metabolically labelled with 4sU for 90 min and total cellular RNA was purified as described in Materials and methods. Changes in mRNA half-lives were calculated for DIS3L2-depleted cells relative to the control. For each condition, three biological replicates of each RNA subset were subjected to qRT-PCR analysis. Error bars calculated as standard error of the mean. * indicates AU-rich mRNAs (ARED3 database; Bakheet *et al*, 2006).

and *S. cerevisiae* cells become inviable only when both activities are simultaneously blocked (Johnson and Kolodner, 1995; Anderson and Parker, 1998). Although mammalian cells contain an hDIS3L-containing and cytoplasm-restricted exosome isoform, insufficient data exist on 3′-5′ cytoplasmic decay in higher eukaryotes, including humans. Here, we reveal a 3′-5′ degradation pathway, which functions in parallel with the cytoplasmic RNA exosome and utilizes a widespread eukaryotic ribonuclease, hDIS3L2 (Figure 7). Unlike in *S. cerevisiae*, where Dis3p is the only major processive RNase present in both the nucleus and the cytoplasm, fission yeast, most plants and worms are endowed with two RNase II/R domain proteins: Dis3 and Dis3L2 (Supplementary Figure S1B, Zhang *et al*, 2010). Only humans, and other *Deuterostomia*, contain hDIS3L (Tomecki *et al*, 2010). However, the Dis3 and Dis3L2 subfamilies are quite distant from each other, while the Dis3L subfamily most likely diverged from Dis3 more recently. The presence of Dis3L2 proteins may have been previously overlooked as the majority of research on cytoplasmic RNA degradation has been performed in *S. cerevisiae*, which does not have an hDIS3L2 homologue. Indeed, during the preparation of this manuscript-independent studies have revealed Dis3L2 to be a prominent cytoplasmic degradation activity (Chang *et al*, 2013; Malecki *et al*, 2013). In *S. pombe*, Dis3L2 participates in mRNA degradation, while in mouse embryonic stem cells it degrades let7 pre-miRNA. Interestingly, both pathways appear to involve 3′end uridylation as an RNA decay signal.

Our study strongly suggests that hDIS3L2 is not a part of the RNA exosome. This is presumably because, in contrast to hDIS3 and hDIS3L, its divergent N-terminus lacks the ability to anchor it to hRRP41. Another characteristic of hDIS3L2 proteins is their extended CSD1, a feature that may help define their substrate recognition and explain why 3′-5′ exonuclease activity of hDIS3L2 shows stronger activity

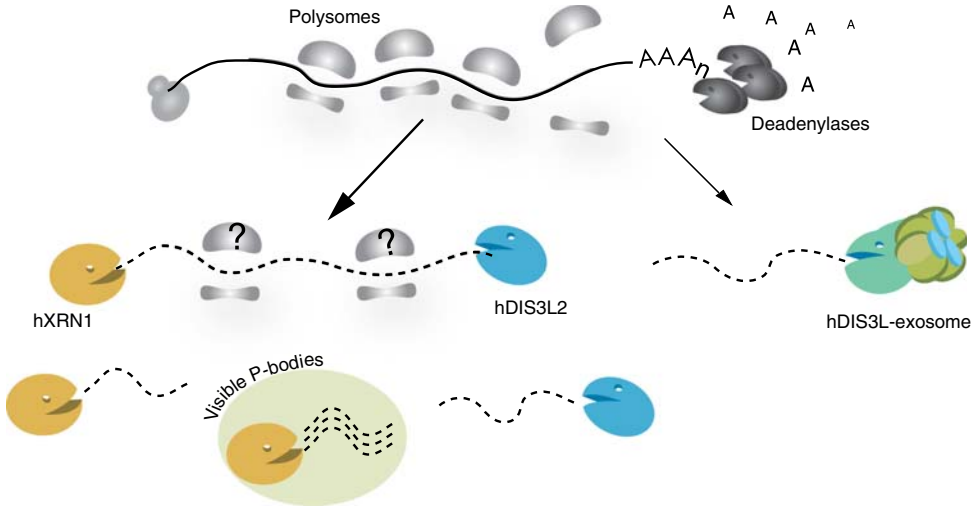


**Figure 7** Schematic model for cytoplasmic mRNA degradation in human cells. The 5′-3′ exonuclease hXRN1, the 3′-5′ exonucleases hDIS3L2, and hDIS3L/exosome impact cytoplasmic mRNA turnover in human cells. A fraction of hXRN1 and hDIS3L2, but not the exosome, associates with ribosomes, however, it remains to be shown whether 3′-5′ degradation also occurs at these assemblies (indicated by question marks). Data indicate that more hXRN1, than hDIS3L2, activity may be localized to visible PBs (see text).

towards structured substrates with short 2 nt overhangs or even blunt-ended dsRNA, when compared to hDIS3 or Dis3p (Figure 2B; Supplementary Figure S2F). hDIS3L2 activity fully depends on its RNB domain with magnesium or manganese ions being essential for catalysis (Figure 2; Supplementary Figure S2). In sum, it therefore appears that hDIS3L2 does not belong to the Dis3 family of exonucleases, but rather is reminiscent of bacterial hydrolytic 3′-5′ exoribonucleases, which usually act as solitary enzymes.

Our data are consistent with hDIS3L2 playing an important role in cytoplasmic mRNA metabolism. Notably, the depletion of hDIS3L2 increases the number of cytoplasmic PBs, which was not observed when depleting the cytoplasmic exosome subunit hDIS3L. It is well known that downregulation of hXRN1 or decapping enzymes leads to an increased size of already existing PBs (Franks and Lykke-Andersen, 2008). In the case of hDIS3L2, its depletion rather increases the number of PBs, which are not significantly larger. Moreover, when hXRN1 and hDIS3L2 are co-depleted populations of both small and large granules are detectable. These effects correlate to some extent with the cytoplasmic localization of the exonucleases; that is, hXRN1 localizes predominantly to PBs (Cougot *et al*, 2004) while hDIS3L2 localizes more uniformly in the cytoplasm. A possibility is, therefore, that hXRN1 depletion primarily nucleates additional PB factors onto existing PBs due to the excess mRNA in these assemblies, whereas hDIS3L2 depletion instead nucleates PB factors on mRNAs normally not associated within microscopically visible PBs. In any case, assuming that both the size and number of PBs correlate with the pool of cytoplasmic mRNA available for aggregation, we conclude that both hDIS3L2 and hXRN1 knockdowns significantly stabilize non-translating mRNAs.

*In vivo*, a role of hDIS3L2 in cytoplasmic mRNA turnover is revealed by its requirement for efficient degradation of an ARE-containing reporter mRNA (β-TNF-α) (Figure 5). The impact of hDIS3L2 on cytoplasmic mRNA metabolism is also supported by our RNAseq experiments as well as connected mRNA half-life analysis. Downregulation of hXRN1, hDIS3L2, or hDIS3L influences the levels of a substantial number of mRNAs and reveals a high degree of redundancy between the three cytoplasmic decay pathways. This pattern is more prominent between hDIS3L2 and hXRN1 depletions, which is in line with the PB phenotypes. All single depletions predominantly accumulate mRNAs encoding proteins involved in cell-cycle regulation. In case of hDIS3L2, this is in agreement with published data showing that hDIS3L2 knockdown leads to increased cell proliferation and decreased chromosomal stability (Astuti *et al*, 2012). Consistent with the observed hDIS3L2 sensitivity of the β-TNF-α reporter, we also find a number of ARE-mRNAs (5%) among hDIS3L2-upregulated transcripts (Bakheet *et al*, 2006). A similar portion of these short-lived transcripts is observed upon hXRN1 and hDIS3L depletions, again exemplifying the redundancy in cytoplasmic RNA decay. There are, however, also hDIS3L2-specific ARE mRNA targets, for example, FZD4. The nature of this specificity remains to be determined. Finally, co-depletion of hXRN1 with hDIS3L2, but not with hDIS3L, results in the strong upregulation of mRNAs encoding transcription regulators as well as a significant downregulation of mRNAs encoding components of the translation apparatus and proteins involved in oxidative phosphorylation (Figure 6C). This implies serious alterations in cell metabolism and could suggest feedback regulation when cytoplasmic mRNA degradation is inhibited. Notably, inactivation of both hDIS3L2 and hXRN1 is lethal in *S. pombe* (Malecki *et al*, 2013).

While mechanistic details of how hDIS3L2 recognizes its substrates remain to be elucidated, our finding that a pool of hDIS3L2 is associated with polysomes suggests that at least some are targeted co-translationally (Figure 7). In this sense, hDIS3L2 may behave similar to hXRN1 and at least to some extent act on the same substrates. The timing and targeting of such 'cooperation' by this new player in cytoplasmic mRNA decay will be the focus of future analysis.

 

## Materials and methods

### *Protein alignments*

Multiple sequence alignments were created using PROMALS3D and protein structures (2id0, 2vnu) from Uniprot and PDB, respectively (Pei *et al*, 2008). The full alignment in Supplementary Figure S1A was visualized in Jalview editor and trimmed in the gap regions (Waterhouse *et al*, 2009). The phylogenetic maximum-likelihood tree was generated based on RNB domain alignments of all hDIS3, hDIS3L, and hDIS3L2 homologues found in the HomoloGene (NCBI) database as well as bacterial RNases used to root the tree. The analysis was carried out on the Mobyle portal using the protpars/protdist (bootstrap = 100) and Archaeopteryx tools (Felsenstein, 1993; Han and Zmasek, 2009).

### *Plasmids*

All plasmids used in the study are listed in Supplementary Table S7. The coding sequence of the longest hDIS3L2 isoform (Q8IYB7, Uniprot) was amplified by PCR using a HeLa cDNA library and oligonucleotides (see Supplementary Table S7), introducing *Bam*HI/*Xho*I restriction sites for cloning into pcDNA5/FRT/TO-FLAG (Invitrogen) and *Bgl*II/*Acc*65I sites for cloning into pEGFP-N1 or -C1, respectively. A tetracycline-inducible cell line stably expressing hDIS3L2-FLAG was generated using the Flp-In™ T-REx™ system (Invitrogen) according to the manufacturer. β-GAPDH and β-TNF-α are generous gifts from Professor Jens Lykke-Andersen, UCSD and has been described elsewhere (Lykke-Andersen *et al*, 2000; Franks and Lykke-Andersen, 2007).

### *RNAi-mediated factor depletion and RT-qPCR analysis*

For siRNA transfections, $0.4 \times 10^5$ HeLa cells were seeded in 100 mm plates. Transfections were carried out using 15 nM siRNA for single depletion (EGFP, hDIS3L, hDIS3L2, and hXRN1) and 10 nM per siRNA for co-depletions (hXRN1/hDIS3L and hXRN1/hDIS3L2) (Supplementary Table S7) for 48 h using SilentFect (Biorad) and repeated for another 48 h using Lipofectamin2000 (Invitrogen). Total RNA was isolated using TRIZOL (Invitrogen) treated with DNase I (Invitrogen), and converted to cDNA by Superscript III using 1 μg of RNA and 100 ng of random primers (according to manufacturer's description). qPCRs were carried out using Platinum SYBR Green (Invitrogen) and 0.2 μM of relevant oligonucleotides (Supplementary Table S7) at an annealing temperature of 60°C on Stratagene Mx3005P.

### *Localization studies*

HEK293 or HeLa cells were seeded onto glass coverslips in 6-well or 12-well plates. For RNAi depletions, the standard transfection protocol was scaled down to fit the experiment. Immunofluorescence analysis was generally performed as described (Tomecki *et al*, 2010). For protein localization in HEK293 cells, the expression of hDIS3L2-FLAG was induced by the addition of 2 ng/ml doxycycline. Twenty-four hours later, cells were fixed and immunolocalization was conducted using polyclonal rabbit α-FLAG (Sigma, 1:700) or polyclonal α-hDIS3L2 (1:500 to 1:1000) antibodies followed by secondary Alexa Fluor 488-conjugated goat anti-rabbit antibodies (1:1000). Imaging was carried out using an Axiovert 200M (Zeiss) epifluorescent microscope equipped with objectives: ×40/0.75 and ×63/1.4 and a coolSNAPHQ camera (Photometrics). For real-time microscopy, cells were transfected with constructs expressing EGFP-tagged hDIS3L2 (N- or C- terminal fusions) and visualized by confocal microscopy (FluoView® FV10i, Olympus, objective ×60/1.2). For localization of PBs, rabbit polyclonal anti-DCP1 antibody was employed (1:1000), followed by secondary antibodies as above. Cell nuclei were visualized by DAPI staining. Quantification of PBs was performed on a randomly selected 150 cells per experiment using the BlobFinder tool (Allalou and Wahlby, 2009). The minimal PB size to merit counting was kept similar for all analyses.

### *Subcellular fractionation*

HeLa cells were seeded in 100 mm plates, transfected as described above and collected in phosphate-buffered saline (PBS) followed by centrifugation at 4°C for 5 min at 500 *g*. After gentle vortexing for 10 s, 1 ml of RSB10 buffer (10 mM Tris/HCl pH 7.4, 10 mM NaCl, 2.5 mM $MgCl_2$), containing digitonin (40 μg/ml) and 1% vanadyl complexes, was added. Cells were vortexed for 10 s, incubated on ice for 5 min and spun at 500 *g* for 5 min at 4°C. Cell supernatants were collected as the soluble cytoplasmic fraction, while the pellet included nuclei and mitochondria.

### *Purification of recombinant hDIS3L2*

His-tagged recombinant hDIS3L2 variants were expressed in *E. coli* and purified on nickel affinity column as previously described (Tomecki *et al*, 2010). The eluates from affinity chromatography steps were separated on an ion exchange column (Resource Q, GE Healthcare) using AKTA purifier FPLC.

### *RNase assays*

*In vitro* hDIS3L2 activity assays were carried out essentially as described (Lorentzen *et al*, 2008; Tomecki *et al*, 2010). Substrates (Supplementary Table S7) were radiolabelled at their 5′ends by polynucleotide kinase using a standard protocol (Sambrook and Russell, 2001), purified by phenol/chloroform and ethanol precipitated. Double-stranded substrates were annealed as previously described (Lorentzen *et al*, 2008). 3′end-labelled and circularized substrates were prepared as described (Tomecki *et al*, 2010). The exception was the RNA substrate presented in Supplementary Figure S2B (ss17-34A), which was labelled with fluorescein instead of $^{32}P$. Proteins were used at a final concentration of 0.1 μM, while substrate concentration was 0.2 and 2 μM for dsRNA and ssRNA, respectively.

### *CoIP experiments*

Expression of hDIS3L2-FLAG was induced with 2 ng/ml of doxycycline for 24 h. As an IP control, an empty host cell line was subjected to a similar treatment. Cells were collected from two 145 mm plates and washed with cold PBS. After gentle centrifugation (500 *g*, 5 min), cell pellets were resuspended in cold lysis buffer (50 mM Tris/HCl pH 8.0, 150 mM NaCl, 2.5 mM $MgCl_2$, 0.5% Triton X-100), containing protease inhibitors (Roche). Cells were lysed by sonication: 3 × 10sek, 20 W (Branson 250) and treated with RNase A (100 μg/ml) for 15 min (on ice). Cell lysates were centrifuged at 16 000 *g* for 15 min at 4°C. For RNase-free experiments, $MgCl_2$ was replaced with 2 mM EDTA and cells were kept on ice without RNAse A. Cleared extracts were loaded onto anti-FLAG (M2) agarose beads (Sigma) and after 90 min of incubation, beads were washed three times with the lysis buffer and twice with the lysis buffer without Triton X-100. Elution was carried out using FLAG peptide (0.5 mg/ml).

For western blotting analysis, 1/10 volume of FLAG eluates was loaded onto 10–12% acrylamide gels. The following antibodies were used: mouse monoclonal α-FLAG (M2, Sigma-Aldrich), rabbit polyclonal α-hDIS3L2 (this study), rabbit polyclonal α-hXRN1 (kind gift from Jens Lykke-Andersen), rabbit polyclonal α-hRRP40 (150662, PTG) rabbit polyclonal α-hRRP6 (P41124, Sigma), and mouse monoclonal α-U1 70K (kind gift from Douglas Black). Anti-mouse and anti-rabbit IgGs conjugated with HRP (Dako) were used as secondary antibodies.

### *MS analyses: sample preparation and data treatment*

Prior to MS analysis, eluates were precipitated with pyrogallol red and digested overnight at 37°C in solution by trypsin (Promega) in 100 mM ammonium bicarbonate buffer. Released peptides were reduced in 10 mM dithiothreitol (DTT) for 30 min and alkylated in 55 mM iodoacetamide for 20 min at room temperature. Finally, trifluoroacetic acid (TFA) was added to a final concentration of 0.1%.

MS and data analyses were performed as previously described (Tomecki, *et al.* 2010). The LTQ-OrbitrapVelos mass spectrometer was operated in a mode, which provides high resolution of ion spectra ($m/z$ 300–1500, resolution 60 000 and ion accumulation to a target value of $5 \times 10^6$ ions). MaxQuant software (version 1.3.0) was used to extract peptide ion and fragment ion $m/z$ intensity signals from the mass spectra (Cox and Mann, 2008), and for database searches (Uniprot species: human reviewed). Data quantitation was performed using the MaxQuant software. Peptide $m/z$ signal intensities were calculated by summing intensities over the entire elution chromatogram of the peptide, and protein intensities were calculated as the sum of intensities for all peptides for the given protein.

### *Polysome gradients*

Polysome profiling was carried out as described (Damgaard and Lykke-Andersen, 2011). Briefly, cells were treated with cycloheximide (100 μg/ml) for 5 min, washed twice with PBS containing cycloheximide and lysed in 1 ml PEB buffer with cycloheximide (50 mM Tris/HCl pH 7.4, 150 mM NaCl, 7.5 mM $MgCl_2$, 0.5% Triton X-100, cycloheximide 100 μg/ml, heparin 500 μg/ml) or without cycloheximide and with EDTA (50 mM Tris/HCl pH 7.4, 150 mM NaCl, 12.5 mM EDTA, 0.5% Triton X-100, heparin 500 μg/ml). After 5 min on ice incubation, extracts were centrifuged for 15 min at 15 000 *g* at 4°C. Polysomes were separated in a 10–50% sucrose gradient by centrifugation at 4°C for 180 min at 35 000 *g* and collected using a Teledyne fraction collector. Proteins were precipitated by incubation with pyrogallol red for 30 min at room temperature and centrifugation for 15 min at 15 000 *g*. Pellets were resuspended in NuPAGE loading buffer with 25 mM DTT and subjected to western blotting analysis.

### *RNA library preparation*

In all, 3 μg of total RNA was depleted for rRNA using Ribo-Zero kit (Epicentre) and cDNA libraries were generated using ScriptSeq v2 kit (EpiCentre) according to manufacturer's instructions. The size distribution and concentration of the cDNA was determined for each library using the Agilent RNA Kit and a Bioanalyzer (Agilent 2100). The protocol is based on random priming and contains size selection steps (Quiagen MiniElute Column purification, AMPure beads purification), which enrich for long RNAs (>200 nt). Consequently, all the libraries were depleted for small RNA, including tRNA and most sn(o)RNA. For sequencing, libraries were pooled according to the barcode indices and sequenced on an Illumina HiScan device. Raw reads were processed on the Galaxy server (Giardine *et al*, 2005), separated by index, subjected to adapter trimming and filtered by quality scores >20 (PHRED scale). The processed reads were aligned to the human reference genome (hg19/GRCh37) using TopHat v1.5.0 (Trapnell *et al*, 2009). HTSeq was used to extract unique exonic reads from mapping files (iGenomes annotations).

### *DEG and GO analysis*

DEGs were identified using DESeq v.1.11.2 according to the manual in R 2.15 environment (http://www.r-project.org/) (Anders and Huber, 2010). DESeq analysis was performed based on dispersion calculated for two biological replicates for all the samples: control, hDIS3L, hDIS3L2 and hXRN1 knockdown. The same approach was used for hDIS3L2/hXRN1 and hDIS3L/hXRN1 knockdowns (data not shown). Normalization was performed based on the upper quartile of each data set. *P*-values were Benjamini Hochberg corrected with threshold for a DEG with false discovery rate <0.05. Functional annotation clustering of the DEG was carried out using DAVID (Huang da *et al*, 2009). Only the significantly enriched GO terms from the biological process category (enrichment score $(-\log(P\text{-value})) > 3$) were visualized.

### *Tetracycline pulse-chase/ northern blotting analysis*

HeLa tet-off cells (Clontech) were transfected as described above at a confluency of 30–40% in 3.5-cm plates. During the second round of transfection, 300 ng of pTET2-BwtB-TNF (reporter—β-TNF-α), 45 ng of pcBwtB-GAP3UAC (internal control—β-GAPDH), and 655 ng of pcDNA3 vector were added to the siRNA transfection mix. In all, 40 ng/ml of tetracycline was included in the medium to inhibit reporter expression. After 24 h, an 8-h transcriptional pulse was initiated by removal of tetracycline and stopped by addition of tetracycline to 1 μg/ml. Cells were collected in subsequent time points (0, 45, 90, and 135 min), starting 30 min after addition of tetracycline. Cell pellets were dissolved in Trizol solution (Invitrogen) and RNA was isolated according to manufacturer's protocol. IN all, 5 μg of total RNA was run on a 1.1% formaldehyde-agarose gel for northern blotting analysis (Sambrook and Russell, 2001) and hybridized with internally $^{32}$P-labelled riboprobes generated by SP6 polymerase-directed *in vitro* transcription of linearized plasmid templates.

### *Calculation of mRNA half-lives based on newly transcribed/ total RNA ratios*

Newly transcribed HeLa cell RNAs were labelled by addition of 4-thiouridine (4sU) to the medium for 90 min at a concentration of 500 μM. Total RNA was isolated and biotinylated as previously described (Dolken *et al*, 2008). 4sU-containing RNA was separated on streptavidin-coated magnetic beads (Dynabeads® MyOne™ Streptavidin T1) under stringent conditions (50 mM Tris/HCl pH 7.4, 1 M NaCl, 1 M Urea, 0.5% Triton X-100, 5 mM EDTA), followed by wash in the same buffer, containing 4 M Urea. RNA was subjected to reverse transcription as described above. Levels of newly synthetized RNAs were measured by qRT-PCR, performed on a fraction of input RNA (total RNA) and eluate from the streptavidin beads (newly transcribed RNA). Relative changes in half-lives were calculated as previously described (Dolken *et al*, 2008). All steps were controlled using in-house *in vitro* transcribed spike-in RNAs containing 4sU.

### *Supplementary data*

Supplementary data are available at *The EMBO Journal* Online (http://www.embojournal.org).

## Acknowledgements

We thank Manfred Schmid and Aleksander Chlebowski for critical reading of the manuscript as well as members of the THJ and AD laboratories for stimulating discussions. We acknowledge Søren Lykke-Andersen and Grzegorz Kudla for experimental advice and thank Krystian Stoduś, Weronika Jonko, Paweł Krawczyk, and Dorota Adamska for their help with protein purification and sample sequencing. Experiments were carried out with the use of CePT infrastructure financed by the European Union—the European Regional Development Fund (Innovative Economy 2007–13). The research was supported by the Danish National Research Foundation, the Danish Cancer Society and the Lundbeck- and Novo Nordisk Foundations (to THJ); The Danish Council for Independent Research and the Lundbeck Foundation (to CD); an NCN Maestro grant (UMO-2011/02/A/NZ1/00001) (to AD) and a Iuventus Plus research grant (IP2010 043470) and a scholarship for outstanding young scientists from the Polish Ministry of Science and Higher Education (to RT). ML was supported by a Boehringer-Ingelheim PhD fellowship and a START fellowship from the Foundation for Polish Science.

*Author contributions*: ML, under supervision of CKD, THJ, and AD, planned and conducted most of the experiments. RT and ML performed biochemical analyses. DC contributed to the MS analysis. ML, THJ, and AD wrote the paper.

## Conflict of interest

The authors declare that they have no conflict of interest.

## References

Allalou A, Wahlby C (2009) BlobFinder, a tool for fluorescence microscopy image cytometry. *Comput Methods Prog Biomed* **94:** 58–65

Allmang C, Kufel J, Chanfreau G, Mitchell P, Petfalski E, Tollervey D (1999) Functions of the exosome in rRNA, snoRNA and snRNA synthesis. *EMBO J* **18:** 5399–5410

Anders S, Huber W (2010) Differential expression analysis for sequence count data. *Genome Biol* **11:** R106

Anderson JS, Parker RP (1998) The 3′ to 5′ degradation of yeast mRNAs is a general mechanism for mRNA turnover that requires the SKI2 DEVH box protein and 3′ to 5′ exonucleases of the exosome complex. *EMBO J* **17:** 1497–1506

Astuti D, Morris MR, Cooper WN, Staals RH, Wake NC, Fews GA, Gill H, Gentle D, Shuib S, Ricketts CJ, Cole T, van Essen AJ, van Lingen RA, Neri G, Opitz JM, Rump P, Stolte-Dijkstra I, Muller F, Pruijn GJ, Latif F *et al* (2012) Germline mutations

 

in DIS3L2 cause the Perlman syndrome of overgrowth and Wilms tumor susceptibility. *Nat Genet* **44:** 277–284

Bakheet T, Williams BR, Khabar KS (2006) ARED 3.0: the large and diverse AU-rich transcriptome. *Nucleic Acids Res* **34:** D111–D114

Balagopal V, Fluch L, Nissan T (2012) Ways and means of eukaryotic mRNA decay. *Biochim Biophys Acta* **1819:** 593–603

Bonneau F, Basquin J, Ebert J, Lorentzen E, Conti E (2009) The yeast exosome functions as a macromolecular cage to channel RNA substrates for degradation. *Cell* **139:** 547–559

Chang HM, Triboulet R, Thornton JE, Gregory RI (2013) A role for the Perlman syndrome exonuclease Dis3l2 in the Lin28-let-7 pathway. *Nature* **497:** 244–248

Chen CY, Gherzi R, Ong SE, Chan EL, Raijmakers R, Pruijn GJ, Stoecklin G, Moroni C, Mann M, Karin M (2001) AU binding proteins recruit the exosome to degrade ARE-containing mRNAs. *Cell* **107:** 451–464

Chen CY, Shyu AB (1995) AU-rich elements: characterization and importance in mRNA degradation. *Trends Biochem Sci* **20:** 465–470

Cheng ZF, Deutscher MP (2002) Purification and characterization of the Escherichia coli exoribonuclease RNase R. Comparison with RNase II. *J Biol Chem* **277:** 21624–21629

Cougot N, Babajko S, Seraphin B (2004) Cytoplasmic foci are sites of mRNA decay in human cells. *J Cell Biol* **165:** 31–40

Cox J, Mann M (2008) MaxQuant enables high peptide identification rates, individualized p.p.b.-range mass accuracies and proteome-wide protein quantification. *Nat Biotechnol* **26:** 1367–1372

Damgaard CK, Lykke-Andersen J (2011) Translational coregulation of 5′TOP mRNAs by TIA-1 and TIAR. *Genes Dev* **25:** 2057–2068

Decker CJ, Parker R (1993) A turnover pathway for both stable and unstable mRNAs in yeast: evidence for a requirement for deadenylation. *Genes Dev* **7:** 1632–1643

Decker CJ, Parker R (2012) P-bodies and stress granules: possible roles in the control of translation and mRNA degradation. *Cold Spring Harb Perspect Biol* **4:** a012286

Dolken L, Ruzsics Z, Radle B, Friedel CC, Zimmer R, Mages J, Hoffmann R, Dickinson P, Forster T, Ghazal P, Koszinowski UH (2008) High-resolution gene expression profiling for simultaneous kinetic parameter analysis of RNA synthesis and decay. *RNA* **14:** 1959–1972

Drazkowska K, Tomecki R, Stodus K, Kowalska K, Czarnocki-Cieciura M, Dziembowski A (2013) The RNA exosome complex central channel controls both exonuclease and endonuclease Dis3 activities *in vivo* and *in vitro*. *Nucleic Acids Res* **41:** 3845–3858

Dziembowski A, Lorentzen E, Conti E, Seraphin B (2007) A single subunit, Dis3, is essentially responsible for yeast exosome core activity. *Nat Struct Mol Biol* **14:** 15–22

Eulalio A, Rehwinkel J, Stricker M, Huntzinger E, Yang SF, Doerks T, Dorner S, Bork P, Boutros M, Izaurralde E (2007) Target-specific requirements for enhancers of decapping in miRNA-mediated gene silencing. *Genes Dev* **21:** 2558–2570

Felsenstein J (1993) *PHYLIP (Phylogeny Inference Package) version 3.5 c*. Distributed by the author. Seattle, WA, USA: Department of Genetics, University of Washington

Fenger-Gron M, Fillman C, Norrild B, Lykke-Andersen J (2005) Multiple processing body factors and the ARE binding protein TTP activate mRNA decapping. *Mol Cell* **20:** 905–915

Franks TM, Lykke-Andersen J (2007) TTP and BRF proteins nucleate processing body formation to silence mRNAs with AU-rich elements. *Genes Dev* **21:** 719–735

Franks TM, Lykke-Andersen J (2008) The control of mRNA decapping and P-body formation. *Mol Cell* **32:** 605–615

Geisler S, Coller J (2012) Chapter Five—XRN1: a major 5′ to 3′ exoribonuclease in eukaryotic cells. In *The Enzymes,* Vol. 31, pp 97–114. NY, USA: Academic Press

Giardine B, Riemer C, Hardison RC, Burhans R, Elnitski L, Shah P, Zhang Y, Blankenberg D, Albert I, Taylor J, Miller W, Kent WJ, Nekrutenko A (2005) Galaxy: a platform for interactive large-scale genome analysis. *Genome Res* **15:** 1451–1455

Goldstrohm AC, Wickens M (2008) Multifunctional deadenylase complexes diversify mRNA control. *Nat Rev Mol Cell Biol* **9:** 337–344

Han MV, Zmasek CM (2009) phyloXML: XML for evolutionary biology and comparative genomics. *BMC Bioinformatics* **10:** 356

Houseley J, Tollervey D (2009) The many pathways of RNA degradation. *Cell* **136:** 763–776

Hsu CL, Stevens A (1993) Yeast cells lacking 5′–>3′ exoribonuclease 1 contain mRNA species that are poly(A) deficient and partially lack the 5' cap structure. *Mol Cell Biol* **13:** 4826–4835

Hu W, Petzold C, Coller J, Baker KE (2010) Nonsense-mediated mRNA decapping occurs on polyribosomes in Saccharomyces cerevisiae. *Nat Struct Mol Biol* **17:** 244–247

Hu W, Sweet TJ, Chamnongpol S, Baker KE, Coller J (2009) Co-translational mRNA decay in Saccharomyces cerevisiae. *Nature* **461:** 225–229

Huang da W, Sherman BT, Lempicki RA (2009) Systematic and integrative analysis of large gene lists using DAVID bioinformatics resources. *Nat Protoc* **4:** 44–57

Johnson AW, Kolodner RD (1995) Synthetic lethality of sep1 (xrn1) ski2 and sep1 (xrn1) ski3 mutants of Saccharomyces cerevisiae is independent of killer virus and suggests a general role for these genes in translation control. *Mol Cell Biol* **15:** 2719–2727

Kedersha N, Stoecklin G, Ayodele M, Yacono P, Lykke-Andersen J, Fritzler MJ, Scheuner D, Kaufman RJ, Golan DE, Anderson P (2005) Stress granules and processing bodies are dynamically linked sites of mRNP remodeling. *J Cell Biol* **169:** 871–884

Korner CG, Wahle E (1997) Poly(A) tail shortening by a mammalian poly(A)-specific 3′-exoribonuclease. *J Biol Chem* **272:** 10448–10456

Lebreton A, Tomecki R, Dziembowski A, Seraphin B (2008) Endonucleolytic RNA cleavage by a eukaryotic exosome. *Nature* **456:** 993–996

Lee G, Bratkowski MA, Ding F, Ke A, Ha T (2012) Elastic coupling between RNA degradation and unwinding by an exoribonuclease. *Science* **336:** 1726–1729

Lorentzen E, Basquin J, Tomecki R, Dziembowski A, Conti E (2008) Structure of the active subunit of the yeast exosome core, Rrp44: diverse modes of substrate recruitment in the RNase II nuclease family. *Mol Cell* **29:** 717–728

Lubas M, Chlebowski A, Dziembowski A, Jensen TH (2012) Chapter One—Biochemistry and function of RNA exosomes. In *The Enzymes,* Vol. 31, pp 1–30. NY, USA: Academic Press

Lubas M, Christensen MS, Kristiansen MS, Domanski M, Falkenby LG, Lykke-Andersen S, Andersen JS, Dziembowski A, Jensen TH (2011) Interaction profiling identifies the human nuclear exosome targeting complex. *Mol Cell* **43:** 624–637

Lykke-Andersen J, Shu MD, Steitz JA (2000) Human Upf proteins target an mRNA for nonsense-mediated decay when bound downstream of a termination codon. *Cell* **103:** 1121–1131

Lykke-Andersen J, Wagner E (2005) Recruitment and activation of mRNA decay enzymes by two ARE-mediated decay activation domains in the proteins TTP and BRF-1. *Genes Dev* **19:** 351–361

Lykke-Andersen S, Tomecki R, Jensen TH, Dziembowski A (2011) The eukaryotic RNA exosome: same scaffold but variable catalytic subunits. *RNA Biol* **8:** 61–66

Makino DL, Baumgartner M, Conti E (2013) Crystal structure of an RNA-bound 11-subunit eukaryotic exosome complex. *Nature* **495:** 70–75

Malecki M, Viegas SC, Carneiro T, Golik P, Dressaire C, Ferreira MG, Arraiano CM (2013) The exoribonuclease Dis3L2 defines a novel eukaryotic RNA degradation pathway. *EMBO J* **32:** 1842–1854

Mangus DA, Jacobson A (1999) Linking mRNA turnover and translation: assessing the polyribosomal association of mRNA decay factors and degradative intermediates. *Methods* **17:** 28–37

Mitchell P, Petfalski E, Shevchenko A, Mann M, Tollervey D (1997) The exosome: a conserved eukaryotic RNA processing complex containing multiple 3′–>5′ exoribonucleases. *Cell* **91:** 457–466

Muhlemann O, Jensen TH (2012) mRNP quality control goes regulatory. *Trends Genet* **28:** 70–77

Muhlrad D, Decker CJ, Parker R (1994) Deadenylation of the unstable mRNA encoded by the yeast MFA2 gene leads to decapping followed by 5′–>3′ digestion of the transcript. *Genes Dev* **8:** 855–866

Pei J, Tang M, Grishin NV (2008) PROMALS3D web server for accurate multiple protein sequence and structure alignments. *Nucleic Acids Res* **36:** W30–W34

Sambrook J, Russell D (2001) *Molecular Cloning: A Laboratory Manual*. 3rd edn, Plainview, New York: Cold Spring Harbor Laboratories

Schaeffer D, Reis FP, Johnson SJ, Arraiano CM, van Hoof A (2012) The CR3 motif of Rrp44p is important for interaction with the core exosome and exosome function. *Nucleic Acids Res* **40:** 9298–9307

Schaeffer D, Tsanova B, Barbas A, Reis FP, Dastidar EG, Sanchez-Rotunno M, Arraiano CM, van Hoof A (2009) The exosome contains domains with specific endoribonuclease, exoribonuclease and cytoplasmic mRNA decay activities. *Nat Struct Mol Biol* **16:** 56–62

Schilders G, van Dijk E, Pruijn GJ (2007) C1D and hMtr4p associate with the human exosome subunit PM/Scl-100 and are involved in pre-rRNA processing. *Nucleic Acids Res* **35:** 2564–2572

Schneider C, Leung E, Brown J, Tollervey D (2009) The N-terminal PIN domain of the exosome subunit Rrp44 harbors endonuclease activity and tethers Rrp44 to the yeast core exosome. *Nucleic Acids Res* **37:** 1127–1140

Schoenberg DR, Maquat LE (2012) Regulation of cytoplasmic mRNA decay. *Nat Rev Genet* **13:** 246–259

Sheth U, Parker R (2003) Decapping and decay of messenger RNA occur in cytoplasmic processing bodies. *Science* **300:** 805–808

Staals RH, Bronkhorst AW, Schilders G, Slomovic S, Schuster G, Heck AJ, Raijmakers R, Pruijn GJ (2010) Dis3-like 1: a novel exoribonuclease associated with the human exosome. *EMBO J* **29:** 2358–2367

Stevens A (1980) Purification and characterization of a Saccharomyces cerevisiae exoribonuclease which yields 5′-mononucleotides by a 5′ leads to 3′ mode of hydrolysis. *J Biol Chem* **255:** 3080–3085

Stoecklin G, Mayo T, Anderson P (2006) ARE-mRNA degradation requires the 5′-3′ decay pathway. *EMBO Rep* **7:** 72–77

Tomecki R, Kristiansen MS, Lykke-Andersen S, Chlebowski A, Larsen KM, Szczesny RJ, Drazkowska K, Pastula A, Andersen JS, Stepien PP, Dziembowski A, Jensen TH (2010) The human core exosome interacts with differentially localized processive RNases: hDIS3 and hDIS3L. *EMBO J* **29:** 2342–2357

Trapnell C, Pachter L, Salzberg SL (2009) TopHat: discovering splice junctions with RNA-Seq. *Bioinformatics* **25:** 1105–1111

Tucker M, Valencia-Sanchez MA, Staples RR, Chen J, Denis CL, Parker R (2001) The transcription factor associated Ccr4 and Caf1 proteins are components of the major cytoplasmic mRNA deadenylase in Saccharomyces cerevisiae. *Cell* **104:** 377–386

Wang Z, Jiao X, Carr-Schmid A, Kiledjian M (2002) The hDcp2 protein is a mammalian mRNA decapping enzyme. *Proc Natl Acad Sci USA* **99:** 12663–12668

Wasmuth EV, Lima CD (2012) Exo- and endoribonucleolytic activities of yeast cytoplasmic and nuclear RNA exosomes are dependent on the noncatalytic core and central channel. *Mol Cell* **48:** 133–144

Waterhouse AM, Procter JB, Martin DM, Clamp M, Barton GJ (2009) Jalview Version 2–a multiple sequence alignment editor and analysis workbench. *Bioinformatics* **25:** 1189–1191

Zhang W, Murphy C, Sieburth LE (2010) Conserved RNaseII domain protein functions in cytoplasmic mRNA decay and suppresses Arabidopsis decapping mutant phenotypes. *Proc Natl Acad Sci USA* **107:** 15981–15985

 